Acta Crystallographica Section B
Structural Science
ISSN 0108-7681

Structure and phase transitions in $Ca_2CoSi_2O_7$–$Ca_2ZnSi_2O_7$ solid-solution crystals

Z. H. Jia,[a] A. K. Schaper,[a]* W. Massa,[b] W. Treutmann[a] and H. Rager[a]

[a]Department of Geosciences, Material Sciences Center, Philipps University Marburg, Hans-Meerwein-Strasse, D-35032 Marburg, Germany, and [b]Department of Chemistry, Material Sciences Center, Philipps University Marburg, Hans-Meerwein-Strasse, D-35032 Marburg, Germany

Correspondence e-mail: schaper@staff.uni-marburg.de

Received 23 December 2005
Accepted 5 May 2006

While the incommensurability in melilites is well documented, the underlying atomic configurations and the composition-dependent phase behavior are not yet clear. We have studied the transition from the incommensurate phase to the high-temperature normal phase (IC-N), and to the low-temperature commensurate phase (IC-C) of selected members of the $Ca_2Co_{1-x}Zn_xSi_2O_7$ system using X-ray and single-crystal electron diffraction, as well as calorimetric measurements. The space group of the unmodulated normal phase and of the basic structure of the incommensurate phase is $P\bar{4}2_1m$; the commensurate lock-in superstructure was refined as a pseudomerohedral twin in the orthorhombic space group $P2_12_12$. We found that the commensurate modulation is mainly connected with a sawtooth-like periodicity of rotations of the T^1 tetrahedra in the 3×3 superstructure. In this structure, the clustering of the low-coordinated Ca^{2+} ions is not complete so that only imperfect octagons were detected. Generally, the effect of increasing substitution of Co by Zn was a continuous reduction of the IC-N and IC-C transition temperatures.

1. Introduction

The average (basic) crystal structure of melilites with the formula $X_2T^1T_2^2O_7$ was originally determined by Warren (1930) and carefully reexamined by Smith (1953) as being of tetragonal space group using a natural Capo di Bove melilite of the composition $(Ca,Na,K)_2(Mg,Al)(Si,Al)_2O_7$. Since then this structure has been confirmed from refinements of the different melilites $Ca_2MgSi_2O_7$ (åkermanite; Kimata & Ii, 1981), $Ca_2ZnSi_2O_7$ (hardystonite; Bindi, Chank, Röthlisberger & Bonazzi, 2001), $Ca_2Al_2SiO_7$ (gehlenite; Kimata & Ii, 1982; Swainson *et al.*, 1992), $Ca_2SiB_2O_7$ (okayamalite; Giuli *et al.*, 2000) and $Ca_2BeSi_2O_7$ (gugiaite; Yang *et al.*, 2001), as well as most of their substitutional variants (see Armbruster *et al.*, 1990; Röthlisberger *et al.*, 1990; Bindi, Bonazzi, Duśek, Petrićek & Chapuis, 2001), examined in either their synthetic or natural form. Clear deviations from the above supercell were observed in a few other melilite-type compounds. Symmetries such as $P2_1$ (low $Ca_2ZnGe_2O_7$; Armbruster *et al.*, 1990), $I\bar{4}$ (meliphanite; Dal Negro *et al.*, 1967), $P2_12_12_1$ (leucophanite; Grice & Hawthorne, 1989) and $C222_1$ (jeffreyite; Grice & Robinson, 1984) have been observed. These lower symmetries are ascribed to the ordering of some of the minor atomic constituents (see also Bindi *et al.*, 2003).

The melilites are prominent examples of the two-dimensional incommensurate modulation in crystals. This modulation is described by the superspace formalism introduced by

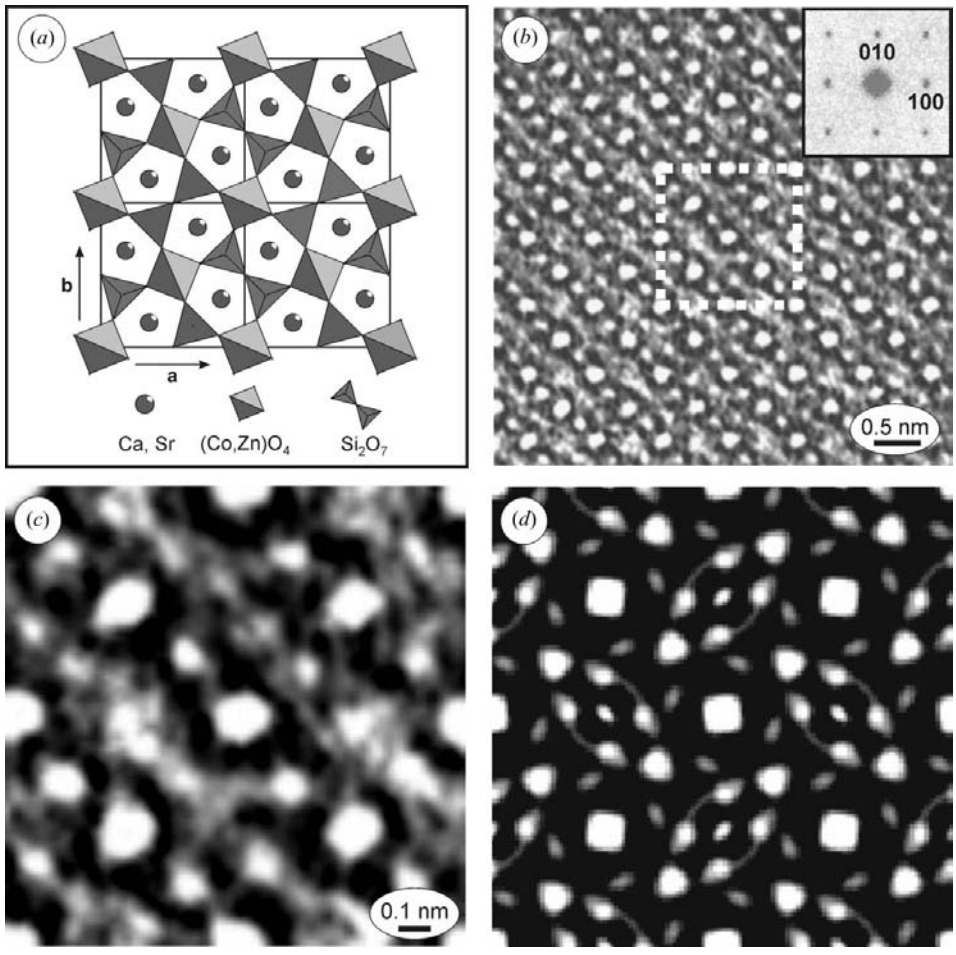

Figure 1
(*a*) Projection on the crystallographic *ab* plane of the basic melilite structure (four unit cells are shown); (*b*) high-voltage, high-resolution transmission electron micrograph of a thin specimen area of a Co-melilite crystal with the Fourier power spectrum inset; (*c*) magnified region squared with the dotted line in Fig. 1(*b*); (*d*) multi-slice image simulation with a defocus value of $\Delta f = 80$ nm and the specimen thickness $t = 3.5$ nm.

de Wolff (1974), Janner & Jansen (1977) and van Smaalen (1987). Much experimental and theoretical work has been carried out in order to clarify the deformation of the basic crystal lattice, the displacement patterns and the corresponding symmetry changes resulting from the misfit between the layers formed by the $[T^1O_4]$ and $[T^2{}_2O_7]$ groups, and the interlayer cations that lead to complex incommensurate modulation regimes (Hemingway *et al.*, 1986; Seifert *et al.*, 1987; Röthlisberger *et al.*, 1990; Van Heurck *et al.*, 1992; Tamura *et al.*, 1996). Particular insight into the fundamental mechanisms of the modulation formation was gained by studying the phase transformational processes toward the non-modulated normal phase (Iishi *et al.*, 1990; Brown *et al.*, 1994; Jiang *et al.*, 1998; McConnell *et al.*, 2000; Schosnig *et al.*, 2000; Kusaka *et al.*, 2001; Kusz & Böhm, 2001; Bindi & Bonazzi, 2005; Merlini *et al.*, 2005) and more specifically into the low-temperature commensurate lock-in phase (Riester & Böhm, 1997; Schosnig *et al.*, 2000; Riester *et al.*, 2000; Hagiya *et al.*, 2001; Bagautdinov *et al.*, 2002; Bindi & Bonazzi, 2003) *via* the variation of temperature and/or chemical composition.

Applying the notation of Janner *et al.* (1983), the five-dimensional superspace group of the incommensurate melilite phase was proposed to be $P\bar{4}2_1m{:}P4mg$ by Hagiya *et al.* (1993). This was also chosen in later studies by Kusaka *et al.* (1998), Bagautdinov *et al.* (2000) and Bindi, Bonazzi, Dušek, Petříček & Chapuis (2001). McConnell (1999), by group-theoretical approaches, and Hagiya *et al.* (2001), by X-ray refinement of Co-åkermanite, found $P\bar{4}$ and $P2_12_12$ as the only suitable subgroups related to the commensurate modulation of the melilites. While the $P\bar{4}$ symmetry was also suggested by Riester *et al.* (2000) for the commensurate lock-in phase of Co-åkermanite below 130 K, Kimata *et al.* (1997) and Hagiya *et al.* (2001) obtained better agreement of the satellite intensities with the orthorhombic $P2_12_12$ group.

The indeterminate situation regarding an adequate description of the modulation structure in melilites has motivated us to perform X-ray and electron microscopy and diffraction, as well as calorimetric measurements of single crystals of the solid-solution series $Ca_2CoSi_2O_7$–$Ca_2ZnSi_2O_7$. Thus, in contrast to our earlier studies of Sr-åkermanites with variations of the *X* cation site (Jiang *et al.*, 1998; Schosnig *et al.*, 2000), here we have studied the case of the varying T^1 site at a fixed *X* cation site. The results of investigations of the incommensurate-to-normal (IC-N) and the incommensurate-to-commensurate (IC-C) phase transition, and of the structure refinement of the commensurate low-temperature lock-in phase in particular are presented. Details of the crystal growth technique and the room-temperature modulation characteristics have been reported elsewhere (Jia *et al.*, 2004).

2. Experimental

$Ca_2Co_{1-x}Zn_xSi_2O_7$ single crystals with $x = 0$, 0.1, 0.3, 0.5, 0.7, 0.9 and 1.0 were synthesized by the floating-zone melting method (for details see Jia *et al.*, 2004). An excess of 1% ZnO

was added to compensate for the evaporation loss of ZnO at high temperature. Thin discs with the *c* axis aligned normal to the disc plane were cut from the bulk crystals and glued into 3 mm diameter special Ti sample holders. The samples were mechanically thinned down to ∼ 50–70 µm and subsequently Ar ion-milled in a TECHNOORG–LINDA Model IV3/H/L apparatus using the high-energy gun (7–8 kV) until perforation appeared. Final polishing of the surfaces was carried out using the low-energy gun operated between 1 kV and 400 V. A JEM 3010 transmission electron microscope (JEOL), equipped with a slow-scan CCD camera (GATAN MegaScan 794) and operated at 300 kV, was used for the electron diffraction measurements along with a GATAN 636-DH double-tilt liquid nitrogen (LN_2) cooling holder for the low-temperature measurements. High-resolution studies were carried out in the high-voltage atomic resolution transmission electron microscope (HVTEM) JEM-ARM1250 (JEOL) at the Max Planck Institute for Metals Research in Stuttgart (Germany), operated at an accelerating voltage of 1250 kV. For multislice image simulation we used the *JEMS* software program (Stadelmann, 2004).

Single-crystal X-ray diffraction measurements were carried out using a STOE IPDS-II imaging-plate diffraction system operating with graphite-monochromated Mo $K\alpha$ radiation. The standard uncertainty of the **q**-vector components was determined using the *X-AREA* program (Stoe & Cie, 2006). An Oxford cryosystem device was used to perform *in situ* cooling experiments down to 100 K. The *SHELXL*97 (Sheldrick, 1997) program package was used for the refinement of the commensurately modulated structure.

Heat-capacity measurements were performed in a Mettler Toledo DSC 821 under nitrogen atmosphere. The sample (7 mg) was placed in a standard aluminium pan. The heating and cooling cycles were applied twice at a rate of 5 K min^{-1}; the second heating curve was used to calculate the phase-transition temperature.

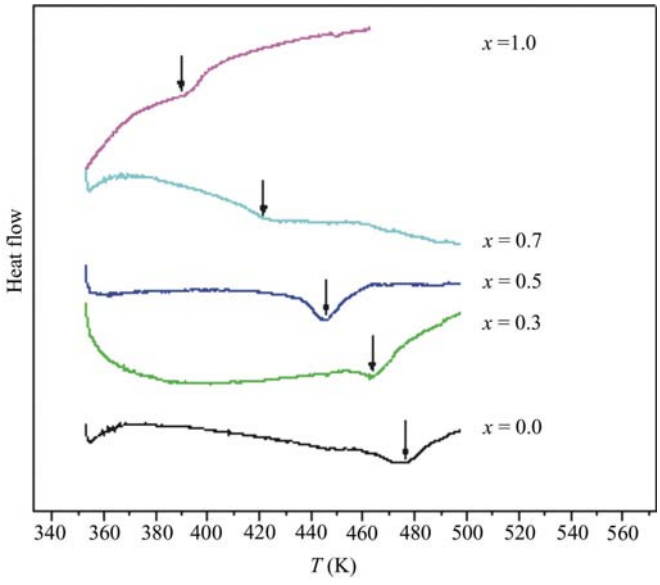

Figure 2
Temperature dependence of the heat capacity of $Ca_2Co_{1-x}Zn_xSi_2O_7$ compounds during phase transition from the incommensurate to the normal structure. Arrows indicate the endothermic second-order peaks.

3. Results and discussion

3.1. The incommensurate-to-normal (IC-N) phase transition

The high-resolution transmission electron micrograph shown in Fig. 1(*b*), taken at 1250 kV of a thin specimen region in a Co end-member crystal, and the corresponding Fourier power spectrum of the image reveal the basic tetragonal structure of the incommensurate melilite phase along the [001] direction, as shown in Fig. 1(*a*). There is an excellent fit of the Ca as well as the Co atom positions if the magnified image in Fig. 1(*c*) is compared with the simulated image in Fig. 1(*d*) for the case of 3.5 nm sample thickness. Si and O are not clearly resolved.

According to the recent analyses by Bindi & Bonazzi (2005) of the natural melilite $(Ca_{1.87}Sr_{0.02}Na_{0.10}K_{0.02})_{\Sigma 2.01}(Mg_{0.96}Al_{0.07})_{\Sigma 1.03}(Si_{1.98}Al_{0.02})_{\Sigma 2.00}O_7$, and by Kusaka *et al.* (2001) of floating zone-grown $Ca_2CoSi_2O_7$, $Ca_2MgSi_2O_7$ and $Ca_2(Mg_{0.55}Fe_{0.45})Si_2O_7$, the normal (unmodulated) high-temperature phase does not significantly differ from the basic structure of the incommensurate phase of the space group $P\bar{4}2_1m$. The dependence of the IC-N transition temperature $T_{IC\text{-}N}$ on composition was determined (see Fig. 2) by measuring the heat-capacity anomaly of $Ca_2Co_{1-x}Zn_xSi_2O_7$ along the range $0.0 \leq x \leq 1.0$. $T_{IC\text{-}N}$ steadily shifts to lower temperature with increasing Zn content and the peaks become broader. No significant differences between the

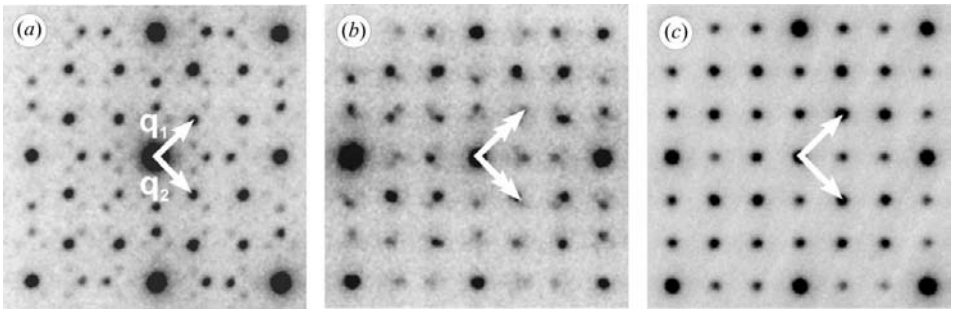

Figure 3
Electron diffraction of $Ca_2Co_{0.9}Zn_{0.1}Si_2O_7$ with changes in temperature: (*a*) incommensurately modulated structure at 297 K with the modulation vectors q_1 and q_2; (*b*) extension of the Bragg reflections along the ⟨110⟩ directions around 168 K, indicating the coexistence of crystal domains still in the incommensurate state, and of domains already transformed into the commensurate lock-in phase; (*c*) (near-) commensurate lock-in structure at 91 K (α = 0.328).

heating and cooling runs were observed; the lack of any hysteresis effect indicates the second-order character of the phase transition. The transition temperatures for the Co and Zn end-members are 478 and 390 K, respectively. These temperatures are a little below the corresponding calorimetric data (493 and 402 K) obtained by Iishi *et al.* (1991), and also below the X-ray value (493 K) of Kusaka *et al.* (2001) for the Co-melilite Both measures, however, match rather well the temperature ranges based on electron-density analyses (483–493 and 373–393 K) given by Röthlishberger *et al.* (1990). The deviations probably arise from the kinetics of the phase transition and from differences in the experimental conditions.

3.2. The incommensurate-to-commensurate (IC-C) transition

Fig. 3 shows the [001] zone-axis electron diffraction patterns at three different temperatures during the *in situ* cooling of a $Ca_2Co_{0.9}Zn_{0.1}Si_2O_7$ single crystal. At 297 K, besides the tetragonal Bragg reflections, first- and second-order satellites of the two-dimensional incommensurate modulation were observed (Fig. 3*a*). Upon lowering the temperature to 168 K, diffuse broadening of the scattering intensity of the satellites was detected along the [110] and [1$\bar{1}$0] modulation directions (Fig. 3*b*), and a proceeding shift of the intensity maxima toward the commensurate position, indicating the successive completion of the IC-C phase transition. At 91 K the whole crystal became transformed into the lock-in phase with the commensurate satellite reflections, and their combinatorial reflections, being almost exactly located at the rational positions $\pm$ 1/3 and $\pm$ 2/3 with respect to the main reciprocal lattice spots (Fig. 3*c*).

Fig. 4 gives a detailed analysis of the modulation vector **q** [$\mathbf{q}_1 = \alpha(\mathbf{a}^* + \mathbf{b}^*)$ and $\mathbf{q}_2 = \alpha(-\mathbf{a}^* + \mathbf{b}^*)$] in an x = 0.1 single crystal with decreasing (run a) and increasing (run b) temperature. In order to approach the thermal equilibration of the structure, every electron-diffraction pattern was taken after holding the temperature at the respective value for 1 h. During the lowering of the temperature, the α value in the incommensurate phase initially remained below 0.30 and did not change considerably until it jumped, over the range 175–130 K, to a plateau value around 0.33. In the opposite direction, at increasing temperature, α dropped down beyond 200 K, with the transition being completed at about 250 K. This observation is evidence of a prominent hysteresis of the phase transition process. In addition, the temperature dependence of the **q** vectors has been determined from X-ray single-crystal diffraction measurements (IPDS-II, Stoe) at 190, 230, 250, 260, 270, 280 and 293 K in the sequence of rising temperature. The results are included in Fig. 4 (run c). The transition interval between the commensurate and the incommensurate phase is shifted by $\sim$ 50 K towards higher temperature compared with electron diffraction. To explain this discrepancy, the much stronger interaction of the electron beam than of X-rays with the sample has to be taken into account as this interaction may activate the structural changes associated with the phase transition. Other reasons to be considered are the differences in the dimensional scales of probing of the two methods and the presence of a domain structure of the crystals. While X-ray diffraction, as an integral method, averages over a volume of the order 0.01 mm^3, the information from electron diffraction is very local and relates to an extremely thin, almost two-dimensional sample disk of a few 100 nm in diameter in the present experiments. Assuming the domain size to be of the order 100 nm or less (Van Heurck *et al.*, 1992; Schaper *et al.*, 2001; Kusaka *et al.*, 2004), electron diffraction provides very selective information from a few single domains only. Hence, if the progress in the phase transition does not occur simultaneously within different domains, electron diffraction may already reveal commensurate behavior, while the majority of the crystal is still in an incommensurate stage as X-ray scattering suggests.

A situation like this, where different phases coexist side by side under quite the same thermodynamic conditions, is proved in Fig. 5. The satellite reflections in Fig. 5(*a*) indicate an incommensurate phase with $\alpha \simeq 0.30$ in one area, but those

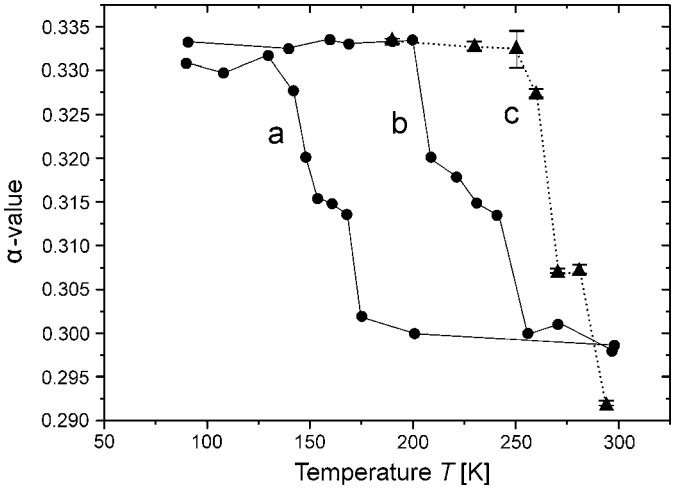

Figure 4
The α value of the modulation **q** vector as a function of temperature for $Ca_2Co_{0.9}Zn_{0.1}Si_2O_7$ determined by electron diffraction at (*a*) decreasing and (*b*) increasing temperature, and (*c*) by X-ray diffraction during heating. (Electron diffraction values were calculated by averaging over five measures; a reasonable estimate for the standard uncertainty is $\pm$ 0.002. The standard uncertainties determined from the X-ray diffraction patterns vary due to the different numbers of frames used.)

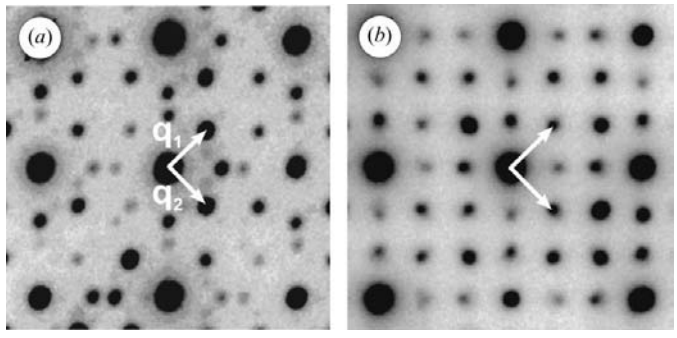

Figure 5
Electron diffraction patterns taken at 130 K of neighboring regions in a $Ca_2CoSi_2O_7$ crystal showing in (*a*) an incommensurate phase with α = 0.301, and in (*b*) a near commensurate phase with α = 0.322.

in Fig. 5(*b*) reveal a near-commensurate lock-in phase with $\alpha \simeq 0.32$ in another area of the same sample; both electron diffraction patterns were taken at 126 K one after the other.

Altogether, in the $Ca_2Co_{1-x}Zn_xSi_2O_7$ system the commensurate phase has been observed at the LN_2 temperature up to a Zn content of $x = 0.3$, as the electron diffraction data in the lower part of Fig. 6 show. The diffraction patterns were taken after prolonged cooling to guarantee that equilibrium had been reached. Measurements at liquid helium (LHe) are required to follow the low-temperature phase transition for $x > 3$, as the diagram indicates. The same tendency of decreasing transition temperature with increasing Zn content was obtained for the IC-N transition; the results for $T_{IC\text{-}C}$ are included in Fig. 6. This behavior, indicating a reduction in the misfit between the tetrahedral layers and the intermediate Ca layer, is in agreement with our previous findings (Jia *et al.*, 2004) of decreasing lattice parameters *a* and *c* with increasing *x* value.

3.3. Refinement of the commensurate lock-in structure

The intensity data were taken from diffraction measurements with the X-ray area detector at 190 K. Refinement of the commensurate modulated structure of $Ca_2Co_{0.9}Zn_{0.1}Si_2O_7$ was performed as a 3×3 superstructure in both the space groups $P\bar{4}$ (as a merohedral twin) and $P2_12_12$ [as a pseudo-merohedral (110) twin]. According to the group-theoretical calculations by McConnell (1999), these space groups are the only suitable subgroups of the basic space group $P\bar{4}2_1m$ related to the modulation of the melilite structure. The parameters of Riester *et al.* (2000) (space group $P\bar{4}$) and of Hagiya *et al.* (2001) (space group $P2_12_12$) for the pure $Ca_2CoSi_2O_7$ compound were used as starting models.

Although all atoms could be refined without any positional constraints in the space group $P\bar{4}$ with the residuals $R_1 = 0.101$ and $wR_2 = 0.195$ for all 8488 reflections [$R_1 = 0.0758$, $wR_2 = 0.1751$ for reflections with $I > 2\sigma(I)$], some of the displacement parameters became non-positive definite. Furthermore, for the heavy Ca and Co atoms, refinement of the anisotropic displacement parameters remained unstable. In the space group $P2_12_12$, however, sensible anisotropic displacement parameters could be refined for all heavy atoms, and for most of the O atoms. Nevertheless, for the final cycles only isotropic parameters were used in order to reduce the total number of parameters. With a ratio of twin domains refined to 0.465 (3) the refinement using all 7239 independent reflections gave much better residuals of $R_1 = 0.0717$ and $wR_2 = 0.1137$, and $R_1 = 0.0526$, $wR_2 = 0.1053$ for the reflections with $I > 2\sigma(I)$. The correct orientation of the structure with respect to the polar axis is documented in a Flack parameter $x = 0.00$ (2). Attempts to refine the Co:Zn ratio on the five Co/Zn sites in order to obtain information on the possible concentration modulation of the Zn contents were not successful. This is not surprising in view of the small difference in scattering power of the two elements. However, also for $Ca_2(Mg_{0.55}Fe_{0.45})Si_2O_7$ with good scattering contrast, the occupational modulation could not be determined by Kusaka *et al.* (1998). On the other hand, in the case of Ca through Sr substitution in $(Ca_{0.96}Sr_{0.04})_2MgSi_2O_7$ we derived indications of an occupancy contribution to the modulation from electron crystallographic analysis (Jiang *et al.*, 1998). Bagautdinov *et al.* (2000) found a sinusoidal occupancy modulation in $(Ca_{0.87}Sr_{0.13})_2CoSi_2O_7$.

The final residual electron density maxima and minima are 0.84/−0.85 e Å^{-3}, much lower than in the $P\bar{4}$ refinement (1.50/−1.20). The rather flat difference-Fourier map, the better residuals in a well converging refinement and the sensitive displacement parameters (U_{eq}/U_{iso} all in the range 0.011–0.022 Å^2) clearly confirm the choice of the orthorhombic space group $P2_12_12$ suggested by Hagiya *et al.* (2001). As in Hagiya's work, no violation of the extinction rules for the space group $P2_12_12$ was observed. In the reflection profiles, no deviation from tetragonal metrics could be recognized, but small differences may be hidden by the twinning. The crystal data and experimental conditions are collected in Table 1.[1] Interatomic distances, measured at 190 K, as well as the average mean calculated from each distance, are given in Table 2. The structure including the atom-labeling scheme is shown in Fig. 7. It remains unclear why, in spite of better residuals and a higher number of reflections, the standard deviations of the bond lengths are worse in our case than that published by Hagiya *et al.* (2001), even if the refinement is made, as in their case, using isotropic displacement parameters to achieve a corresponding number of parameters [our data: $R = 0.0584$ for 5777 reflections ($I > 2\sigma(I)$), $R = 0.0774$ for all 7239 reflections, 219 parameters; Hagiya's data: $R = 0.084$ for 6152 reflections $> 1.5\sigma(I)$, 217 parameters]. Perhaps the calculation of the standard uncertainty is different in the *SHELXL* program and in the *HITLST* program used by Hagiya *et al.* (2001).

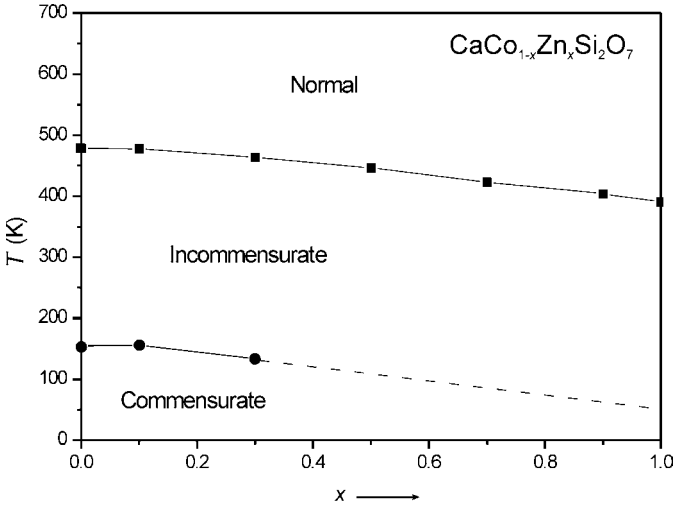

Figure 6
Stability regions of the different phases in the $Ca_2Co_{1-x}Zn_xSi_2O_7$ system depending on composition and temperature. (Extrapolation of the $T_{IC\text{-}C}$ values toward lower temperatures is indicated by a dotted line.)

[1] Supplementary data for this paper, including the results from the refinement of the alternative space group $P\bar{4}$, are available from the IUCr electronic archives (Reference: CK5015). Services for accessing these data are described at the back of the journal.

Table 1
Crystal data and measurement conditions of $Ca_2Co_{09}Zn_{01}Si_2O_7$.

Crystal data	
Chemical formula	$Ca_2Co_{0.90}O_7Si_2Zn_{0.10}$
M_r	307.91
Cell setting, space group	Orthorhombic, $P2_12_12$
Temperature (K)	190 (2)
a, b, c (Å)	23.518 (1), 23.518 (1), 5.0263 (3)
V (Å^3)	2780.0 (2)
Z	18
D_x (Mg m^{-3})	3.311
Radiation type	Mo $K\alpha$
No. of reflections for cell parameters	25 736
θ range (°)	1.7–30.9
μ (mm^{-1})	4.93
Crystal form, colour	Platelet, blue
Crystal size (mm)	0.15 × 0.12 × 0.02
Data collection	
Diffractometer	IPDS-II (Stoe)
Data collection method	ω scans
Absorption correction	Numerical
T_{min}	0.598
T_{max}	0.907
No. of measured, independent and observed reflections	22 026, 7239, 5777
Criterion for observed reflections	$I > 2\sigma(I)$
R_{int}	0.080
θ_{max} (°)	29.0
Range of h, k, l	$-30 \Rightarrow h \Rightarrow 31$ $-32 \Rightarrow k \Rightarrow 31$ $-6 \Rightarrow l \Rightarrow 6$
Refinement	
Refinement on	F^2
$R[F^2 > 2\sigma(F^2)]$, $wR(F^2)$, S	0.053, 0.114, 1.10
No. of reflections	7239
No. of parameters	332
Weighting scheme	$w = 1/[\sigma^2(F_o^2) + (0.040P)^2 + 1.20P]$, where $P = (F_o^2 + 2F_c^2)/3$
$(\Delta/\sigma)_{max}$	0.00
$\Delta\rho_{max}$, $\Delta\rho_{min}$ (e Å^{-3})	0.84, −0.85
Extinction method	*SHELXL*
Extinction coefficient	0.0010 (1)
Absolute structure	Flack (1983), 3076 Friedel pairs
Flack parameter	0.00 (12)

Computer programs used: *XAREA 1.2* (Stoe & Cie, 2003), *SHELXL*97 (Sheldrick, 1997), *DIAMOND* (Crystal Impact, 2005).

There are nine independent Si tetrahedra in the 3 × 3 superlattice cell. The mean Si—O distances range between 1.620 and 1.646 Å. As expected, the longer ones are found in the Si—O—Si bridges.

For the five independent Co(Zn) atoms in the 3 × 3 superstructure the (Co, Zn)–O distances vary between 1.921 (8) and 1.971 (7) Å, *i.e.* over a range which is less than that calculated for the incommensurate modulated structure of the pure Co compound at 297 K (1.908–1.999 Å; Kusaka *et al.*, 2001). The T^1O_4 tetrahedra are distorted and rotated to different degrees, as depicted in Fig. 8. The Co,Zn(5) tetrahedron in particular is strongly flattened along the [001] direction; the two angles O24—(Co,Zn)5—O32 = 127.8° and O29—(Co,Zn)5—O25 = 125.6° are considerably larger than the regular tetrahedral angle of 109.47°. The most striking feature in the lock-in phase compared with the basic structure is the distinct rotation pattern of formerly translationally identical T^1 tetrahedra. In Fig. 8 the rotation angles are marked that are formed by the *a* axis and the projection of a suitable (Co,Zn)—O bond of each tetrahedron onto the (001) plane. If the rotation angles are noted along a row of formerly identical tetrahedra, for instance along the *a* axis (Co1, Co4, Co4*a*, Co1′...), a sawtooth-like periodicity is observed (Fig. 9).

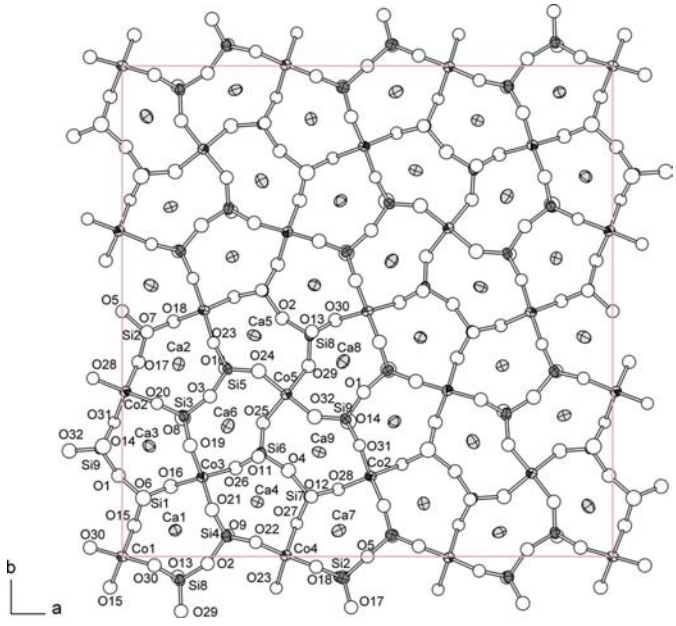

Figure 7
The commensurate lock-in structure of $Ca_2Co_{0.9}Zn_{0.1}Si_2O_7$ determined at 190 K. All atoms of the asymmetric unit are labeled.

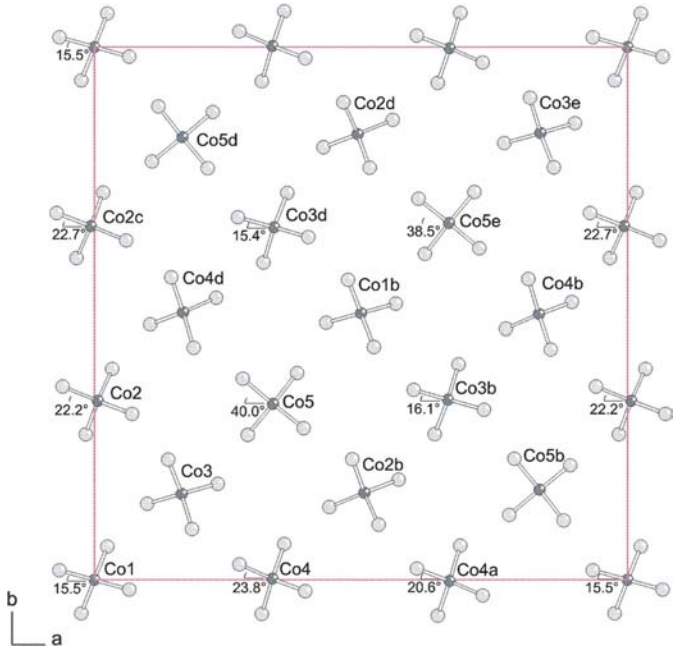

Figure 8
[001] projection of the T^1 tetrahedra of the commensurate lock-in structure of $Ca_2Co_{0.9}Zn_{0.1}Si_2O_7$. The angles formed by the projection of a Co—O bond and the *a* axis are given.

Table 2
Bond lengths (Å) in $Ca_2Co_{09}Zn_{01}Si_2O_7$ at 190 K.

(Co,Zn)1—O15^{i}	1.944 (9)	(Co,Zn)2—O20	1.940 (8)	(Co,Zn)3—O19	1.949 (9)
(Co,Zn)1—O15^{ii}	1.944 (9)	(Co,Zn)2—O17^{ii}	1.954 (8)	(Co,Zn)3—O16^{ii}	1.959 (9)
(Co,Zn)1—O30^{iii}	1.952 (9)	(Co,Zn)2—O31^{iv}	1.961 (8)	(Co,Zn)3—O26^{ii}	1.966 (8)
(Co,Zn)1—O30^{v}	1.952 (9)	(Co,Zn)2—O28^{iii}	1.966 (8)	(Co,Zn)3—O21	1.970 (8)
Mean	1.948	Mean	1.955	Mean	1.961
(Co,Zn)4—O18^{v}	1.921 (8)	(Co,Zn)5—O24	1.926 (8)		
(Co,Zn)4—O22	1.932 (8)	(Co,Zn)5—O32	1.927 (8)		
(Co,Zn)4—O23	1.954 (8)	(Co,Zn)5—O29^{ii}	1.955 (7)		
(Co,Zn)4—O27^{ii}	1.955 (8)	(Co,Zn)5—O25^{ii}	1.971 (7)		
Mean	1.941	Mean	1.945		
Si1—O6	1.578 (12)	Si2—O7	1.601 (8)	Si3—O8^{ii}	1.585 (11)
Si1—O16^{ii}	1.612 (9)	Si2—O18^{ii}	1.615 (9)	Si3—O20	1.622 (8)
Si1—O15^{ii}	1.632 (9)	Si2—O17^{ii}	1.624 (8)	Si3—O19	1.629 (9)
Si1—O1^{ii}	1.659 (8)	Si2—O5^{iv}	1.661 (5)	Si3—O3	1.657 (8)
Mean	1.620	Mean	1.625	Mean	1.623
Si4—O9^{ii}	1.621 (10)	Si5—O10^{ii}	1.617 (10)	Si6—O11	1.601 (8)
Si4—O22	1.635 (9)	Si5—O24	1.621 (8)	Si6—O25^{ii}	1.611 (7)
Si4—O21	1.644 (9)	Si5—O23	1.649 (8)	Si6—O25^{ii}	1.619 (8)
Si4—O2	1.682 (9)	Si5—O3	1.675 (8)	Si6—O4^{ii}	1.658 (8)
Mean	1.646	Mean	1.641	Mean	1.622
Si7—O12	1.594 (9)	Si8—O13	1.591 (10)	Si9—O14^{ii}	1.578 (11)
Si7—O27^{ii}	1.635 (9)	Si8—O29^{ii}	1.609 (8)	Si9—O32	1.603 (8)
Si7—O28^{ii}	1.635 (8)	Si8—O30^{ii}	1.637 (9)	Si9—O31	1.650 (9)
Si7—O4^{ii}	1.680 (8)	Si8—O2^{vii}	1.675 (9)	Si9—O1^{viii}	1.668 (9)
Mean	1.636	Mean	1.628	Mean	1.625
Ca1—O15	2.397 (9)	Ca2—O17	2.387 (8)	Ca3—O19	2.400 (9)
Ca1—O30^{v}	2.428 (9)	Ca2—O23	2.426 (8)	Ca3—O31^{iii}	2.452 (8)
Ca1—O21	2.429 (9)	Ca2—O18	2.481 (9)	Ca3—O8	2.458 (10)
Ca1—O13^{v}	2.533 (8)	Ca2—O7	2.512 (8)	Ca3—O20	2.498 (8)
Ca1—O6	2.535 (11)	Ca2—O10	2.524 (9)	Ca3—O14^{iii}	2.529 (9)
Ca1—O16	2.536 (9)	Ca2—O20	2.539 (8)	Ca3—O16	2.607 (9)
Ca1—O2	2.758 (8)	Ca2—O3	2.682 (8)	Ca3—O1	2.612 (9)
Ca1—O9	2.842 (9)	Ca2—O8	2.902 (10)	Ca3—O6	2.825 (10)
Ca4—O22	2.389 (8)	Ca5—O24	2.306 (8)	Ca6—O25	2.298 (7)
Ca4—O26	2.409 (8)	Ca5—O2^{vi}	2.347 (8)	Ca6—O11	2.412 (8)
Ca4—O9	2.446 (9)	Ca5—O23	2.404 (8)	Ca6—O3	2.431 (7)
Ca4—O11	2.479 (8)	Ca5—O10	2.452 (9)	Ca6—O26	2.476 (9)
Ca4—O27	2.579 (9)	Ca5—O9^{vi}	2.480 (8)	Ca6—O8	2.492 (11)
Ca4—O21	2.610 (9)	Ca5—O22^{vi}	2.554 (8)	Ca6—O19	2.529 (9)
Ca4—O4	2.675 (10)	[Ca5—O13	2.973 (8)]	[Ca6—O10	2.962 (9)]
Ca4—O12	2.884 (9)				
Ca7—O28	2.391 (8)	Ca8—O29	2.286 (8)	Ca9—O32	2.345 (8)
Ca7—O27	2.457 (8)	Ca8—O13	2.430 (8)	Ca9—O31	2.388 (8)
Ca7—O5	2.458 (8)	Ca8—O30	2.433 (9)	Ca9—O14	2.401 (9)
Ca7—O12	2.471 (8)	Ca8—O15^{viii}	2.438 (9)	Ca9—O4	2.418 (9)
Ca7—O18^{v}	2.502 (9)	Ca8—O1^{viii}	2.438 (10)	Ca9—O12	2.452 (9)
Ca7—O7^{v}	2.553 (9)	Ca8—O6^{viii}	2.531 (11)	Ca9—O28	2.493 (8)
Ca7—O7^{viii}	2.847 (9)	[Ca8—O14	3.106 (9)]	[Ca9—O11	3.123 (8)]
Ca7—O17^{viii}	2.876 (9)				

Symmetry codes: (i) $-x, -y, z-1$; (ii) $x, y, z-1$; (iii) $x-\frac{1}{2}, -y+\frac{1}{2}, -z+1$; (iv) $x-\frac{1}{2}, -y+\frac{1}{2}, -z$; (v) $-x+\frac{1}{2}, y-\frac{1}{2}, -z+1$; (vi) $-x+\frac{1}{2}, y+\frac{1}{2}, -z+1$; (vii) $-x+\frac{1}{2}, y+\frac{1}{2}, -z$; (viii) $x+\frac{1}{2}, -y+\frac{1}{2}, -z+1$.

This is the case in all parallel rows ($y = 0, \frac{1}{3}, \frac{2}{3}$) along the [100] direction, but also in the [010] direction ($x = 0, \frac{1}{3}, \frac{2}{3}$). Similar behavior has been derived recently by Michiue *et al.* (2005) for the incommensurate crystallographic shear structure of $Ba_xB_{2-2x}Ti_{4-x}O_{11-4x}$ ($x = 0.275$). This type of torsional deformation of the tetrahedra is a point of view not yet considered, but it may provide a starting point for future refinement approaches with the aid of alternative modulation functions. Under the reasonable assumption of correlations between the structure of the lock-in phase and the incommensurate modulated phase, sawtooth functions seem to provide a more adequate description of the modulation. Moreover, the observation of twinning in the lock-in phase points to the possibility that the incommensurate phase also has to be treated as a twin.

The Ca—O bond length exhibits large variations with the consequence that, considering a critical bond length of Ca—O $\leq$ 2.9 Å, Ca can be assigned to be of six- (Ca5, Ca6, Ca8, Ca9), seven- (Ca2) or eightfold (Ca1, Ca3, Ca4, Ca7) coordination (see Fig. 7). The low-coordinated Ca ions are grouped in bundles along the *c* axis, as shown in Fig. 10. A similar pattern was found by Hagiya *et al.* (2001) for the pure Co compound. The arrangement of the bundles is quite different from that of the model of Riester *et al.* (2000), where the T^1 tetrahedra related to six-coordinated Ca were proposed to form octagonal clusters. In our case, only overlapping $\frac{3}{4}$ fragments of octagons can be localized.

4. Conclusions

This study has shown that the IC-N and IC-C phase transitions in $Ca_2CoSi_2O_7$–$Ca_2ZnSi_2O_7$ solid solutions shift, with increasing Zn for Co substitution, to lower temperatures. This means a reduction of the structural misfit between the tetrahedral layers and the intermediate *X* cation layer and decreasing distortion of the T^1O_4 tetrahedra. While the IC-N transition is of second order, the first-order IC-C transition is accompanied by a fundamental variation in the α value of the modulation vector experimentally determined to be $\mathbf{q} = 0.298\ (2)\ (\pm\ \mathbf{a}^* + \mathbf{b}^*)$ at 295 K and $\mathbf{q} = 0.331\ (2)\ (\pm\ \mathbf{a}^* + \mathbf{b}^*)$ at 90 K. The IC-C transition process does not occur simultaneously over the whole crystal, but shows a pronounced hysteresis within a defined temperature and time interval. The commensurate lock-in structure has been refined as a twin in the orthorhombic space group $P2_12_12$ rather than $P\bar{4}$. A sawtooth-like rotational scheme of the T^1O_4 tetrahedra might be the result of energy

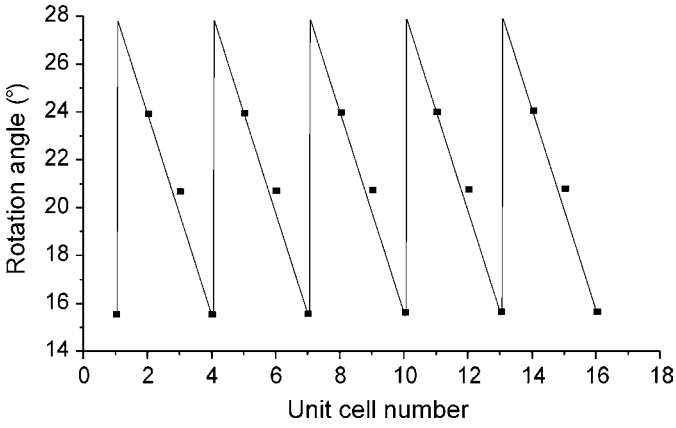

Figure 9
Sawtooth-like modulation function of the rotational angle of the [CoO_4] tetrahedra with respect to the crystallographic *a* axis.

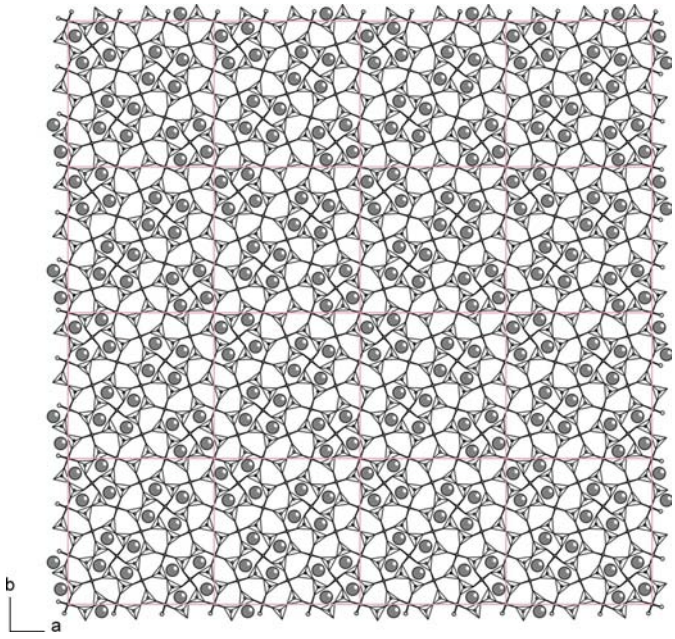

Figure 10
Clustering of the low-coordinated Ca atoms (Ca 5, 6, 8, 9) in [001] projection.

minimization during the commensurate modulation formation and seems to represent a state not far from equilibrium.

Financial support by the German Research Foundation (DFG) within the frame of the Priority Program 1056 'Structural gradients in crystals' is gratefully acknowledged. We thank F. Phillipp, Max Planck Institute for Metals Research, Stuttgart, for his cooperation using high-voltage electron microscopy.

References

Armbruster, Th., Röthlisberger, F. & Seifert, F. (1990). *Am. Mineral.* **75**, 847–858.
Bagautdinov, B., Hagiya, K., Kusaka, K., Ohmasa, M. & Iishi, K. (2000). *Acta Cryst.* B**56**, 811–821.
Bagautdinov, B., Hagiya, K., Noguchi, S., Ohmasa, M., Ikeda, N., Kusaka, K. & Iishi, K. (2002). *Phys. Chem. Miner.* **29**, 346–350.
Bindi, L. & Bonazzi, P. (2003). *Phys. Chem. Miner.* **30**, 523–526.
Bindi, L. & Bonazzi, P. (2005). *Phys. Chem. Miner.* **32**, 89–96.
Bindi, L., Bonazzi, P., Dušek, M., Petrićek, V. & Chapuis, G. (2001). *Acta Cryst.* B**57**, 739–746.
Bindi, L., Chank, M., Röthlisberger, F. & Bonazzi, P. (2001). *Am. Mineral.* **86**, 747–751.
Bindi, L., Rees, L. H. & Bonazzi, P. (2003). *Acta Cryst.* B**59**, 156–158.
Brown, N. E., Ross, C. R. & Webb, S. L. (1994). *Phys. Chem. Miner.* **21**, 469–480.
Crystal Impact (2005). *DIAMOND*, Version 3.0d. Crystal impact, Bonn, Germany.
Dal Negro, A., Rossi, G. & Ungaretti, L. (1967). *Acta Cryst.* **23**, 260–264.
Flack, H. D. (1983). *Acta Cryst.* A**39**, 876–881.
Giuli, G., Bindi, L. & Bonazzi, P. (2000). *Am. Mineral.* **85**, 1512–1515.
Grice, J. D. & Hawthorne, F. C. (1989). *Can. Mineral.* **27**, 193–197.
Grice, J. D. & Robinson, G. W. (1984). *Can. Mineral.* **22**, 443–446.
Hagiya, K., Kusaka, K., Ohmasa, M. & Iishi, K. (2001). *Acta Cryst.* B**57**, 271–277.
Hagiya, K., Ohmasa, M. & Iishi, K. (1993). *Acta Cryst.* B**49**, 172–179.
Hemingway, B. S., Evans, H. T., Nord, G. L., Haselton, H. T., Robie, R. A. & McGee, J. J. (1986). *Can. Mineral.* **24**, 425–434.
Iishi, K., Fujino, K. & Furukawa, Y. (1990). *Phys. Chem. Miner.* **17**, 467–471.
Iishi, K., Mizota, T., Fujino, K. & Furukawa, Y. (1991). *Phys. Chem. Miner.* **17**, 720–725.
Janner, A. & Jansen, T. (1977). *Phys. Rev. B*, **15**, 643–658.
Janner, A., Jansen, T. & Wolff, P. M. de (1983). *Acta Cryst.* A**39**, 658–666.
Jia, Z. H., Schaper, A. K., Treutmann, W., Rager, H. & Massa, W. (2004). *J. Cryst. Growth*, **273**, 303–310.
Jiang, J. C., Schosnig, M., Schaper, A. K., Ganster, K., Rager, H. & Tóth, L. (1998). *Phys. Chem. Miner.* **26**, 128–134.
Kimata, M. & Ii, N. (1981). *Neues Jahrb. Miner. Monatsh.* pp. 1–10.
Kimata, M. & Ii, N. (1982). *Neues Jahrb. Miner. Abh.* **144**, 254–267.
Kimata, M., Saito, S., Shimizu, M. & Nishida, N. (1997). Proc. 17th European Crystallographic Meeting, ECM-17, Lisboa, Portugal, 24–28 August, P3.9–14, p. 156.
Kusaka, K., Hagiya, K., Ohmasa, M. & Iishi, K. (2004). *Acta Cryst.* B**60**, 369–374.
Kusaka, K., Hagiya, K., Ohmasa, M., Okano, Y., Mukai, M., Iishi, K. & Haga, N. (2001). *Phys. Chem. Miner.* **28**, 150–166.
Kusaka, K., Ohmasa, M., Hagiya, K., Iishi, K. & Haga, N. (1998). *Mineral. J.* **20**, 47–58.
Kusz, J. & Böhm, H. (2001). *Z. Kristallogr.* **216**, 509–512.
McConnell, J. D. C. (1999). *Z. Kristallogr.* **214**, 457–464.
McConnell, J. D. C., McCammon, C. A., Angel, R. J. & Seifert, F. (2000). *Z. Kristallogr.* **215**, 669–677.
Merlini, M., Gemmi, M. & Artioli, G. (2005). *Phys. Chem. Miner.* **32**, 189–196.
Michiue, Y., Yamamoto, A., Onoda, M., Sato, A., Akashi, T., Yamane, H. & Goto, T. (2005). *Acta Cryst.* B**61**, 145–153.
Riester, M. & Böhm, H. (1997). *Z. Kristallogr.* **212**, 506–509.
Riester, M., Böhm, H. & Petrićek, V. (2000). *Z. Kristallogr.* **215**, 102–109.
Röthlisberger, F., Seifert, F. & Czank, M. (1990). *Eur. J. Mineral.* **2**, 585–594.
Schaper, A. K., Schosnig, M., Kutoglu, A., Treutmann, W. & Rager, H. (2001). *Acta Cryst.* B**57**, 443–448.

Schosnig, M., Schaper, A. K., Kutoglu, A., Treutmann, W. & Rager, H. (2000). *Z. Kristallogr.* **215**, 495–498.
Seifert, F., Czank, M., Simons, B. & Schmahl, W. (1987). *Phys. Chem. Miner.* **14**, 26–35.
Sheldrick, G. M. (1997). *SHELXS*97. University of Göttingen, Germany.
Smaalen, S. van (1987). *Acta Cryst.* A**43**, 202–207.
Smith, J. V. (1953). *Am. Mineral.* **38**, 643–661.
Stadelmann, P. A. (2004). *JEMS*, ems java version, CIME-EPFL, CH-1015 Lausanne, Switzerland, http://cimewww.epfl.ch/people/stadelmann/jemsWebSite/jems.html.
Stoe & Cie (2003). *XAREA*, Version 1.2. Stoe & Cie GmbH, Darmstadt, Germany.
Stoe & Cie (2006). Test version of modul RECIPE in the *X-AREA* program. Stoe & Cie GmbH, Darmstadt, Germany.
Swainson, I. P., Dove, M. T., Schmahl, W. W. & Putnis, A. (1992). *Phys. Chem. Miner.* **19**, 185–195.
Tamura, T., Yoshiaca, A., Iishi, K., Takeno, S., Maeda, H., Emura, S. & Koto, K. (1996). *Phys. Chem. Miner.* **23**, 81–88.
Van Heurck, C., Van Tendeloo, G. & Amelinckx, S. (1992). *Phys. Chem. Miner.* **18**, 441–452.
Warren, B. E. (1930). *Z. Kristallogr.* **74**, 131–138.
Wolff, P. M. de (1974). *Acta Cryst.* A**30**, 777–795.
Yang, Z. M., Fleck, M., Pertlik, F., Tillmanns, E. & Tao, K. J. (2001). *Neues Jahrb. Mineral. Monatsh.* **4**, 186–192.